Single Electron Spin Decoherence by Nuclear Spin Bath: Linked Cluster Expansion Approach.

S. K. Saikin,[1,2,*] Wang Yao,[1] and L. J. Sham[1]

[1]*Department of Physics, University of California San Diego*

[2]*Department of Physics, Kazan State University, Russia*

(Dated: February 6, 2008)

Abstract

We develop a theoretical model for transverse dynamics of a single electron spin interacting with a nuclear spin bath. The approach allows a simple diagrammatic representation and analytical expressions of different nuclear spin excitation processes contributing to electron spin decoherence and dynamical phase fluctuations. It accounts for nuclear spin dynamics beyond conventional pair correlation models. As an illustration of the theory, we evaluated the coherence dynamics of a P donor electron spin in a Si crystal.

I. INTRODUCTION

An electron-nuclear spin coupling substantially affects electron spin dynamics in solids. This phenomenon is broadly utilized in EPR probing of material structures.[1] However, for novel technological applications of electron spins[2,3] it produces a major obstacle even at low temperatures when effects of phonons are suppressed.[4,5,6,7,8] In particular, it is crucial for a quantum coherence that is a key issue of a quantum computation.[2] Entanglement of an electron spin with a nuclear spin bath results in an irreversible loss of coherence. Unlike spin relaxation,[7] decoherence process is not suppressed even in strong magnetic fields. There are several methods to reduce effects of spin bath, such as isotope purification,[9] dynamical polarization of nuclear spins or dynamical decoupling of an electron spin evolution.[10] However, it is not clear if experimentally achievable values of isotope purification, nuclear polarization or precision of electron spin control are sufficient to suppress effects of spin bath beyond the required threshold limit.[11] Moreover, for some technologically-important materials these methods may be inapplicable. For example, isotope purification cannot be used in GaAs nanostructures, because all stable isotopes of it have non-zero nuclear spins. In this connexion theoretical models of electron-nuclear spin dynamics can provide better understanding of electron spin decoherence processes and also help in estimating the effectiveness of coherence control schemes.

In this work we investigate dynamics of a localized electron spin interacting with a nuclear spin bath at a low temperature regime. We chose a system with a long spin relaxation time that is of interest to quantum computing. Until recently, this problem has been studied using stochastic models of spectral diffusion.[12,13,14] Their results were verified by numerous experiments carried out on macroscopic samples. Recently, emphasis of experimental and theoretical studies has been shifted to dynamics of single quantum systems, where stochastic models are inappropriate. Several analytical and numerical approaches based on quantum dynamics have been developed and used to investigate different aspects of the problem.[15,16,17,18,19,20,21,22,23,24,25,26,27,28,29] Among the issues addressed in these studies are spin relaxation at low external fields,[17,18] effects of nuclear spin polarization on electron spin dynamics,[29] dynamical control for spin decoherence,[28] contributions of high order nuclear spin correlations into an electron spin echo,[27] etc. However, many questions are still open. How do stochastic and dynamical models relate to each other? How does one char-

acterize short time qubit evolution?[30] What are the reversible and irreversible parts of spin dynamics?[31] What are the relative contributions of different correlated nuclear spin clusters in electron spin dynamics? How do nuclear spin correlations grow in time?[32]

Here, we demonstrate that diagram techniques developed previously in studies of Heisenberg ferromagnets[33,34,35,36,37,38,39,40,41] can be applied to evaluate effects of a nuclear spin bath on a single electron spin in a high field regime. Our theoretical approach provides a transparent representation of different nuclear spin dynamical processes contributing to an electron spin evolution. It naturally accounts for nuclear spin excitations beyond pair correlation models. We show that transverse evolution of an electron spin can be factorized to a precession in a nuclear Overhauser field and more complex dynamics due to electron-nuclear spin entanglement.[25] A conventional Hahn echo experiment cancels the phase due to precession in the nuclear field and also suppresses entanglement with the nuclear bath. As an illustration, we consider dynamics of an electron spin localized at phosphorous donor impurity in a Si crystal. We estimate contributions of 2, 3 and 4 nuclear spin excitations to electron spin decoherence and discuss effects of Hahn echo on spin decoherence.

The structure of the paper is as follows. In the next section we describe a Hamiltonian and discuss assumptions used. Section III is devoted to diagrammatic representation of the decoherence process. In Section IV we discuss the approach and consider an example of P donor electron spin in a Si crystal. Section V gives the conclusion. In Appendix A we provide the spin diagrammatic rules, in Appendix B we discuss some specific properties of the linked cluster expansion for spin systems and in Appendix C we give explicit analytical expressions of some high order nuclear spin contributions to electron spin dynamics.

II. MODEL

We consider the spin of a single electron localized in a quantum dot or bounded by a donor impurity. We assume that only one type of nuclear spins with $I = 1/2$ is presented, though this assumption can be relaxed within the approach used. In a strong external magnetic field the Hamiltonian for a single electron spin coupled by the contact hyperfine

interaction[42] with a system of nuclei can be written as

$$H = \omega_e S^z - \omega_I \sum_i I_i^z + S^z \sum_i A_i^{\text{hf}} I_i^z + 2S^z \sum_{i \neq j} B_{ij}^{\text{hf}} I_i^+ I_j^- + \sum_{i \neq j} \{A_{ij}^{\text{dd}} I_i^z I_j^z + B_{ij}^{\text{dd}} I_i^+ I_j^-\}. \quad (1)$$

A similar Hamiltonian has been used in previous studies of the spectral diffusion problem.[23,25] Here, we briefly describe the notations and assumptions. The first two terms in Eq. (1) account for electron and nuclear Zeeman energy level splittings in an external field, H, with the Larmor frequencies $\omega_e = g^*\beta H/\hbar$ and $\omega_I = \gamma H$ respectively. The z-axis is chosen along the magnetic field. The third and fourth terms originate from the contact hyperfine interaction. In a strong magnetic field direct electron-nuclear flip-flop transitions, $(S^+ I_i^- + S^- I_i^+)$, are forbidden by the energy conservation law. Therefore, beside a small visibility loss,[24] this part of the contact interaction contributes to the effective coupling between nuclear spins only.[25] The coupling coefficients are $A_i^{\text{hf}} = (8/3)\pi g_e \beta \gamma |\Psi(R_i)|^2$ and $B_{ij}^{\text{hf}} = A_i^{\text{hf}} A_j^{\text{hf}}/2\omega_e$, where $g_e = 2$ and g^* are free and effective electron g-factors, β is a Bohr magneton, γ is a nuclear γ-factor and $\Psi(R_i)$ is an electron wave function at a position of i-th nuclear spin. The last term in Eq. (1) represents the secular part of the nuclear spin dipole-dipole interaction. For the electron nuclear hyperfine interaction, we consider here only the isotropic contact part. Effects of the dipolar e-n hyperfine interaction, resulting in spin echo envelope modulation,[43,44,45,46] has been discussed elsewhere.[47] The Hamiltonian (1) is diagonal in the electron spin. Therefore, the nuclear spin bath affects transverse electron spin dynamics only.

The initial state of the electron spin plus the system of nuclear spins is described by the density matrix $\rho(0)$ at the time moment, $t = 0$, when the electron spin state has been prepared. Two assumptions are applied to $\rho(0)$. First, we use the standard approximation of a factorized system and bath,[48] $\rho(0) = \rho_s^0 \otimes \rho_n^0$. The electron spin is initially prepared in the pure state, $(1/\sqrt{2})(|+\rangle + |-\rangle)$, e.g., by a $\pi/2$ pulse. The second assumption is that the nuclear spin system is in a pure state that is an eigenstate of $\sum_i I_i^z$ operator. With the latter statement we neglect by nuclear spin-spin correlations at $t < 0$. Influence of different initial states of nuclear bath on electron spin evolution has been discussed in Refs. 19 and 22 though the lack of nuclear spin-spin interaction in these papers may affect their conclusions. It has been argued that the pure spin state utilized here can be useful for quantum computation purposes because it does not destroy electron spin coherence at

short timescales. After statistical averaging over possible initial configurations the nuclear spin density matrix is $\rho_n^0 = \sum p_n |n\rangle\langle n|$, where p_n is a statistical weight of a given nuclear configuration $|n\rangle = |\uparrow\uparrow\downarrow\uparrow\downarrow\downarrow\,...\rangle$.

The evolution of the up-down component $(+-)$ of an electron spin density matrix can be written as[25]

$$\rho_{+-}(t) = \rho_{+-}^0 e^{-i\omega_e t}\mathrm{Tr}_n\{e^{-i(H_0+V_+)t}\rho_n^0 e^{i(-H_0+V_-)t}\},\tag{2}$$

where

$$
\begin{aligned}
H_0 &= (1/2)\sum_i A_i^{\mathrm{hf}} I_i^z,\\
V_\pm &= V_{\mathrm{dd}} \pm V_{\mathrm{hf}},\\
V_{\mathrm{dd}} &= \sum_{i\neq j}\{A_{ij}^{\mathrm{dd}} I_i^z I_j^z + B_{ij}^{\mathrm{dd}} I_i^+ I_j^-\}\\
V_{\mathrm{hf}} &= \sum_{i\neq j} B_{ij}^{\mathrm{hf}} I_i^+ I_j^-.
\end{aligned}\tag{3}
$$

Here, we used the fact that the Hamiltonian (1) commutes with S_z and projected it to the electron spin-up $(+)$ and spin-down $(-)$ subspaces. The projected operators are written as two terms, H_0, which is a sum of single spin operators, and $V_\pm$, which describes spin-spin interactions. A contribution of the nuclear Zeeman splitting, the second term in Eq. (1), is cancelled, because it commutes with the rest of the Hamiltonian. If the nuclear Larmor frequency, ω_I, varies from a site to site due to inhomogeneity of the external field or other factors then its fluctuating part should be included into H_0. Below, we will keep the superscript indexes, (hf) and (dd), in the coupling constants only if it is not clear from the context what type of interaction is used.

Using the relations

$$
\begin{aligned}
e^{-i(H_0+V_+)t} &= T\{e^{-i\int_0^t V_+(t'-t)dt'}\}e^{-iH_0 t},\\
e^{-i(H_0-V_-)t} &= e^{-iH_0 t}T\{e^{i\int_0^t V_-(t')dt'}\},
\end{aligned}\tag{4}
$$

where $T\{...\}$ is a time ordering operator, and our assumption on the initial nuclear spin density matrix, Eq. (2) is transformed to

$$\rho_{+-}(t) = \rho_{+-}^0 e^{-i\omega_e t}\sum_n p_n e^{-i\omega_n t}\langle n|T\{e^{i\int_0^t V_-(t')dt'}\}T\{e^{-i\int_0^t V_+(t'-t)dt'}\}|n\rangle,\tag{5}$$

5

where $\omega_n = \langle n|2H_0|n\rangle$ is a contribution of a nuclear Overhauser field to the electron spin precession frequency and $V_\pm(t)$ is $V_\pm$ in an interaction picture defined by H_0. For a single shot measurement of a single electron spin the nuclear bath contributes to the shift of the electron precession frequency, ω_n, determined by the initial configuration, and complicated dynamics due to coupling between nuclear spins that is described by the bracket $\langle n|...|n\rangle$. The weight factor, p_n, corresponds to a statistical averaging over an ensemble of electron spins or repeated measurements. For an ensemble measurement, Eq. (5) describes a free induction decay,[42] where the transverse magnetic moment decays due to an inhomogeneous distribution of spin precession frequencies and also due to spectral diffusion in the presence of nuclear spin environment. Eq. (5) can be viewed as an exact formal solution for the electron spin dynamics. In following sections we will evaluate the term in it between the angular brackets using the Linked Cluster Expansion (LCE) formalism.[49,50]

In Eq. (5) the product of two exponential operators can be transformed to a single exponential form, $T\{e^{-i\int_{-t}^{t}\tilde{V}(t')dt'}\}$, by shifting the time variable $t'-t \to t'$ in the second exponent. One can see that in this case the potential, $\tilde{V}(t')$, is continuous for the hyperfine-mediated interaction given by Eq. (3), while for the dipole-dipole nuclear spin-spin interactions it changes sign at $t' = 0$. To avoid operations with discontinuous potentials we will use a two-exponential form of a bracket in Eq. (5) keeping in mind that it can be transformed to a single exponent.

Schematically, the bracket in Eq. (5) can be shown as a two branch propagation, Fig. 1. The system propagates on a first branch with the Hamiltonian $V_+(t' - t)$ and after that on a second branch with $-V_-(t')$. This is similar to the non-equilibrim Green's function approach.[51,52]

The factorization of nuclear spin induced dynamics to the phase factor acquired in the nuclear Overhauser field and complex dynamics due to entanglement between bath modes is consistent with EPR experiments. For example, see Ref. 53, where an electron spin resonance line broadening can be resolved to inhomogeneous and homogeneous parts.

The above procedure also can be applied to evaluate electron spin dynamics in experiments where the electron spin is flipped by magnetic pulses. For example, for a Hahn spin

echo ($\pi/2 - t - \pi - t-$ echo) the evolution equation can be written as

$$\rho_{+-}(2t) = -\rho_{-+}^0 \sum_n p_n \langle n|T\{e^{i\int_0^t V_+(t-t')dt'}\}T\{e^{i\int_0^t V_-(t')dt'}\}T\{e^{-i\int_0^t V_+(t'-t)dt'}\}T\{e^{-i\int_0^t V_-(-t')dt'}\}|n\rangle.$$

(6)

We emphasize that the phase factor due to precession in the external field plus the nuclear field that appears in Eq. (5) is cancelled for the echo. Moreover, the bracket $\langle n|...|n\rangle$ describing electron-nuclear spin entanglement is different from the one in Eq. (5). These features correspond respectively to elimination of inhomogeneous broadening and suppression of spectral diffusion in ensemble measurements.[42]

III. LCE AND DECOHERENCE

Using LCE, we can write the expectation value of a time ordered exponent as[49,50]

$$\langle n|T\{e^{\int_0^t V(t')dt'}\}|n\rangle = e^{\langle V_1\rangle + \langle V_2\rangle + \langle V_3\rangle + \cdots},$$

(7)

where $V(t')$ is an interaction and $\langle V_k\rangle$ is a contribution of *linked* diagrams[50] only to the integral

$$\int_0^t dt_1 \int_0^t dt_2 ... \int_0^t dt_k \langle n|T\{V(t_1)V(t_2)...V(t_k)\}|n\rangle.$$

(8)

The coefficient, $1/k$, that appears in LCE, is included in the $\langle V_k\rangle$ terms. This expansion provides a convenient exponential form to describe the dynamical processes. Moreover, each perturbation term $\langle V_k\rangle$ in it corresponds to an infinite sum of terms in a conventional perturbation theory.

The bracket in the expression (8) can be evaluated by a diagrammatic technique. The term $\langle V_k\rangle$ in Eq. (7) is of the k-th order in the interaction. It describes the collective dynamics of a cluster containing up to k spins. Because the proof of LCE can be given based on combinatorics,[50] the expansion procedure should be applicable to potentials, discontinuous in time, or to products of several evolution operators given in Eqs. (5)-(6).

Diagrammatic rules for spins are not so transparent as for fermions or bosons, because commutation brackets of spin operators do not yield c-numbers. Many papers addressed this

issue.[34,35,36,37,38,39,40,41] In our derivations we use the technique described in Refs. 37,38,41 with modifications accounting for specifics of the problem. A brief summary of this technique and the used diagrammatic representations is given in Appendix A.

The LCE expansion of the scattering matrix (7) can be described by the same series of diagrams as a free energy in Matsubara formalism given in Ref. 38. The two-exponential representation of the scattering matrix in Eq. (5) does not change the structure of the diagram series, but affects the spin propagators only. In Figs. 2-4 we show the sets of diagrams corresponding to the bracket in Eqs. (5,6) up to the fourth order in the nuclear spin-spin interaction.

We first discuss the scenario where the nuclear dynamics starts from a pure initial states. Ensemble results are obtained by taking statistical average of all possible initial configurations. Dynamics of each distinct configuration of spins in a cluster, in general, should be depicted by a different diagram specifying an initial spin configuration and the time arrow as it is shown in Fig. 2. However, in many cases analytical expressions for these configurations can be transformed to each other, as is discussed in Appendix A. To reduce the number of diagrams, in the figures we omit the configuration dependence, assuming that one diagram represents all possible configurations. In analytical and numerical evaluations we calculate contributions of distinct spin clusters. We also drop the time arrow for simplicity.

To evaluate diagrams given in Figs. 2-4 we use a 2×2 matrix (matrix elements indexing branches, Fig. 1) Green's function at an i-th site

$$\mathbf{K}^i(\tau) = e^{i\omega_i \tau} \begin{pmatrix} \delta_{i\downarrow}\theta(-\tau) - \delta_{i\uparrow}\theta(\tau) & \delta_{i\downarrow}e^{-i\omega_i t} \\ -\delta_{i\uparrow}e^{i\omega_i t} & \delta_{i\downarrow}\theta(-\tau) - \delta_{i\uparrow}\theta(\tau) \end{pmatrix}, \quad (9)$$

where $\omega_i = A_i^{\mathrm{hf}}/2$ and $\tau = t_1 - t_2$. The total evolution time, t, appears in the off-diagonal elements of $\mathbf{K}^i(\tau)$. Matrix elements of the Green's function (9) possess a simple physical meaning. The propagator starts at time t_1 on a branch denoted by a row index and ends at time t_2 on a branch denoted by a column index. To account for the two-branch propagation the spin-spin coupling coefficients, $A_{ij}^{\mathrm{dd}}, B_{ij}^{\mathrm{dd}}$ should be multiplied by a σ_z Pauli matrix ($\mathbf{A}_{ij}^{\mathrm{dd}} = A_{ij}^{\mathrm{dd}}\sigma_z$, $\mathbf{B}_{ij}^{\mathrm{dd}} = B_{ij}^{\mathrm{dd}}\sigma_z$) and B_{ij}^{hf} should be multiplied by a 2×2 unity matrix ($\mathbf{B}_{ij}^{\mathrm{hf}} = B_{ij}^{\mathrm{hf}}\mathbf{1}$). In the analytical expressions for the diagrams one has to sum over repeating matrix indexes in addition to integration over the time variables.

The first order linked cluster diagram corresponds to $\langle n|\mathbf{A}_{ij}^{\mathrm{dd}} I_i^z I_j^z|n\rangle$ (not shown in Figs. 2-

4). However, its contribution vanishes because the sum over the branches is equal to $\text{Tr}\{\mathbf{A}_{ij}^{\text{dd}}\} = 0$. The first non-zero contribution to the decoherence process is due to the second order diagrams which represents a nuclear pair spin flips, Fig. 2. The corresponding analytical expressions are

$$\langle V_2^{\text{hf}} \rangle = - \sum_{i=\uparrow,j=\downarrow} (B_{ij}^{\text{hf}})^2 \{ \frac{2it}{\omega_{ij}} + \frac{1 - e^{2i\omega_{ij}t}}{\omega_{ij}^2} \}, \tag{10}$$

for the hyperfine-mediated interaction only, and

$$\langle V_2^{\text{dd}} \rangle = - \sum_{i=\uparrow,j=\downarrow} (B_{ij}^{\text{dd}})^2 \{ \frac{2it}{\omega_{ij}} + 4\frac{1 - e^{i\omega_{ij}t}}{\omega_{ij}^2} - \frac{1 - e^{2i\omega_{ij}t}}{\omega_{ij}^2} \}, \tag{11}$$

for the dipole-dipole interaction only, where we define $\omega_{ij} = \omega_i - \omega_j$. This result is consistent with Ref. 25. The real parts of Eqs. (10,11) contribute to electron spin decoherence while the imaginary parts renormalize electron spin precession frequency and, hence, produce phase fluctuations. The $\langle V_2 \rangle$ diagram with a cross-term, $B^{\text{hf}} B^{\text{dd}}$, contribution of the dipole-dipole and hyperfine-mediated interactions is zero because the spin propagators over different branches cancel each other. Therefore, within the second order the contributions of these two mechanisms to electron spin dynamics are completely separable.

We emphasize that in comparison with a conventional perturbation expansion LCE converges faster. Each order in LCE corresponds to an infinite sum of terms. For example, the second order correction in LCE is a partial sum shown in Fig. 5. It includes a series of even orders of a perturbation expansion.

The third order diagrams in Fig. 3 can be divided into two groups. First group includes diagrams 3(a), 3(b) and corresponds to $\langle V_2 \rangle$ diagram with attached $I_i^z I_j^z$ interaction lines. Diagrams of this type can be accounted for by renormalization of Green's functions with the standard equation, Fig. 6, where renormalized Green's function (bold line) is

$$\mathbf{K}^i(t_1, t_2) = e^{i\omega_i \tau} \begin{pmatrix} e^{i\Delta\omega_i \tau}(\delta_{i\downarrow}\theta(-\tau) - \delta_{i\uparrow}\theta(\tau)) & \delta_{i\downarrow} e^{-i\omega_i' t} e^{i\Delta\omega_i \theta} \\ -\delta_{i\uparrow} e^{i\omega_i' t} e^{-i\Delta\omega_i \theta} & e^{-i\Delta\omega_i \tau}(\delta_{i\downarrow}\theta(-\tau) - \delta_{i\uparrow}\theta(\tau)) \end{pmatrix}, \tag{12}$$

$\tau = t_1 - t_2$, $\theta = t_1 + t_2$, $\omega_i' = \omega_i + \Delta\omega_i$ and $\Delta\omega_i = \sum_j A_{ji}\langle I_j^z \rangle$. This modifies the dipole-dipole

pair flip-flop term, Eq. (11), as

$$\langle V_2^{\mathrm{ren}} \rangle = - \sum_{i=\uparrow, j=\downarrow} (B_{ij}^{\mathrm{dd}})^2 \{ \frac{it}{\omega_{11}} + \frac{it}{\omega_{22}} + \frac{1 - e^{i\omega_{11}t}}{\omega_{11}^2} + \frac{1 - e^{i\omega_{22}t}}{\omega_{22}^2} + \frac{(1 - e^{i\omega_{11}t})(1 - e^{i\omega_{22}t})}{\omega_{11}\omega_{22}} \}, \quad (13)$$

where $\omega_{11} = \omega_{ij} + \Delta\omega_i - \Delta\omega_j$ and $\omega_{22} = \omega_{ij} - \Delta\omega_i + \Delta\omega_j$. If we assume that $\Delta\omega_i$ is independent on the site, then Eq. (13) transforms back to Eq. (11). Therefore, the contribution of these renormalization terms is reduced if the initial polarization of the nuclear spin bath is homogeneous. A similar modification of the pair flip-flop term can be due to an inhomogeneous distribution of nuclear Larmor frequencies, ω_I in Eq. (1). The diagram Fig. 3(a) contributes to renormalization of a pair dynamics by $I^z I^z$ interaction. By direct evaluation one can show that for the dipole-dipole interaction it is also cancelled .

The second group of diagrams, Fig. 3(c), is due to three-spin flip-flop processes. It corresponds to a ring propagation of a spin excitation. For the dipole-dipole interaction only, due to symmetry of interaction terms, the clockwise propagating excitation cancels the counterclockwise excitation. It is an analog of the Furry's theorem.[54] An analytical form of the hyperfine-mediated contribution can be written as

$$\langle V_3^{\mathrm{hf}} \rangle = - \sum_{\uparrow\downarrow\downarrow} B_{ij} B_{jk} B_{ki} \{ \frac{4it}{\omega_{ij}\omega_{ik}} - 2\frac{1 - e^{i\omega_{ik}t}}{\omega_{ik}^2\omega_{jk}} + 2\frac{1 - e^{i\omega_{ij}t}}{\omega_{ij}^2\omega_{jk}} \}, \quad (14)$$

for clusters $\{i =\uparrow, j =\downarrow, k =\downarrow\}$, where permutation of j and k spins is included already. For $\{i =\downarrow, j =\uparrow, k =\uparrow\}$ clusters, one should change signs at frequencies $\omega_{i,j,k}$.

In the third order linked diagrams, an effect of cross-terms including both hyperfine-mediated and dipole-dipole interactions appears. For example, a ring diagram, Fig. 3(c) and diagram Fig. 3(a) with two dipole-dipole interaction lines and one hyperfine-mediated line have non-zero contributions. Because most of the third order diagrams give zero contribution to spin decoherence, the fourth order corrections should be evaluated.

The set of the fourth order diagrams is given in Fig. 4. The only restriction on vertices in this diagrams is that two spins i and j coupled by an interaction line should be different $(i \neq j)$. Therefore, the same diagram in Fig. 4 can correspond to different number of spins in a cluster. For example, the ring diagram, Fig. 4(f), can describe excitations of two, three and four spins. We call them two, three and four-spin ring diagrams respectively.

In the fourth order in addition to different types of renormalizations of lower order diagrams, Fig. 4(a-e), and a ring diagram, Fig. 4(f) , we have contribution of locked diagrams,[39] Fig. 4(g,h). By locked diagrams we mean diagrams containing vertices with two incoming propagators. This group compensates overlapping of spin pair excitations and also restricts excitation within a spin space $I^z = \pm 1/2$. The three-spin diagram, Fig. 4(g) modifies a double excitation with one common spin, that appear in expansion of the exponent of V_2 term, and also correct the fourth order ring diagram with repeating indexes, see Fig. 7. The two-spin diagrams Fig. 4(g) and Fig. 4(h) plays a similar role for pairs with two common spins, Fig. 8. In more details we discuss this in Appendix B.

For spin $I = 1/2$ two-spin diagram is compensated completely by the locked diagrams, see Fig. 8(b). The tree spin rings describe dynamics of $i =\uparrow j =\downarrow k =\downarrow$ or $i =\downarrow j =\uparrow k =\uparrow$ clusters. After correction by the locked diagram, Fig. 7(b), it corresponds to propagation of a spin excitation as $i \rightarrow j \rightarrow k \rightarrow j \rightarrow i$. An analytical form of this term together with locked diagrams, Fig. 4(g,h) are given in Appendix C. A four spin ring diagram correspond to dynamics of three distinct spin clusters $\uparrow\downarrow\downarrow\downarrow$, $\uparrow\downarrow\uparrow\downarrow$ and $\uparrow\uparrow\downarrow\downarrow$.

As a result, up to the fourth order in nuclear spin-spin interactions we write equation for the electron spin coherence as

$$\rho_{+-}(t) = \rho_{+-}^0 e^{-i(\omega_e+\omega_n)t} e^{\langle V_2 \rangle_n + \langle V_3 \rangle_n + \langle V_4 \rangle_n}, \tag{15}$$

where the index n denote an initial configuration of the nuclear bath, the $\langle V_2 \rangle_n$ term (diagram on Fig. 2) is given by Eqs. (10,11), the $\langle V_3 \rangle_n$ term (diagram on Fig. 3(c)) with expression given by Eq. (14) and the fourth order contribution of nuclear spin dynamics schematically shown in Fig. 9. Analytical expressions for some terms of $\langle V_4 \rangle_n$ are in Appendix C.

The diagram series can be extended to higher orders. At each order there should be a group of diagrams renormalizing lower orders with $I^z I^z$ terms, a group of locked diagrams that compensate overlapping of spin excitations in lower order clusters, and also a group of ring diagrams.

For systems with a high concentration of nuclear spins, contributions of different diagrams to a $\langle V_k \rangle$ term can be estimated based on $1/Z$ expansion[55], where Z is an effective number of interacting spins. For example, if the last term in Fig. 9 is O(1), then the first term is O($1/Z$), second term is O($1/Z$) or O($1/Z^2$) depending on whether the diagram cor-

responds to a three or two-spin cluster, and the third one is O$(1/Z^2)$. This follows directly from counting of a number of summands (different spin configurations) in the analytical expressions, Appendix C. If the effective number of spins interacting with a given one is large then $\langle V_4 \rangle$ term can be approximated by the last diagram in Fig. 9 only.

IV. DISCUSSION AND EXAMPLE

The equation for a free evolution of a single electron spin coupled with a nuclear bath, Eq. (15), contains two terms. First one is a phase factor due to spin precession in the external field plus the Overhauser field. The second term is due to electron-nuclear spin entanglement. In ensemble measurements, the inhomogeneous distribution of the nuclear Overhauser fields typically leads to a fast ensemble dephasing time T_2^*. This complicates direct observation of spin decoherence in FID. To remove the undesired phase factor one can use, for example, a Hahn spin-echo setup. However, it should be noted that the magnetic π pulse affects the entanglement term also.[25] All the terms evaluated in the previous section can be calculated for the echo setup straightforwardly. For example, the second order term with the dipole-dipole interaction, Fig. 2, is

$$\langle V_2^{\mathrm{dd}} \rangle = - \sum_{i=\uparrow, j=\downarrow} (B_{ij}^{\mathrm{dd}})^2 \{ 12 \frac{1 - e^{i\omega_{ij}t}}{\omega_{ij}^2} + 4 \frac{1 - e^{-i\omega_{ij}t}}{\omega_{ij}^2} - 4 \frac{1 - e^{2i\omega_{ij}t}}{\omega_{ij}^2} \}. \tag{16}$$

Moreover, all the diagrams with the hyperfine-mediated interaction are cancelled for the echo.

As an example we apply the developed technique to a model system, a phosphorous donor in a Si crystal, that was first studied long ago.[53] Recently, interest in it has been renewed by a proposal for quantum computation.[56] The ^{31}P is a shallow donor with the effective radius of the electron wave function $R_{\mathrm{eff}} \sim 25$Å.[57] Therefore, the bounded electron covers many host lattice sites. The nuclear spin bath is represented by a system of randomly distributed ^{29}Si isotopes ($I = 1/2$). The natural ^{29}Si isotope concentration is $c(^{29}\mathrm{Si}) \approx 4.7\%$. At temperatures ~ 1K and magnetic fields $\sim 0.1 - 1$T the major mechanism of spin echo decay in this system is a nuclear spin spectral diffusion.[9,13]

We simulated numerically the processes shown in Figs. 2,9 for a single FID ($\pi/2 - t-$ measurement) and spin echo setup ($\pi/2 - t/2 - \pi - t/2-$ measurement). For FID we factorize

the shift due to the nuclear Overhauser field out and concentrate only on the decoherence induced by electron-nuclear dynamical entanglement. Such calculation becomes relevant when the inhomogeneous broadening can be filtered out, e.g., by the method discussed in Ref. 58. The contact hyperfine constants for the system were approximated using the effective mass theory envelop function.[57] We also assumed that the phosphorus nuclear spin contributes to the frequency shift only, because of large difference in $\gamma-$factors of ^{31}P and ^{29}Si nuclei. In simulations of dipole-dipole contributions we generated an initial nuclear spin configuration in a Si lattice within a sphere of radius $5R_{\rm eff}$ about the donor. Nuclear spin bath was assumed un-polarized. Then we selected randomly a spin-up site with its surrounding within a sphere of a radius $5a$, where $a = 5.43\mathring{A}$ is a Si lattice constant. We calculated contributions of all possible configurations of a given central spin with its surrounding. This procedure was repeated for 10^3 times and results were normalized to the total number of spin-up within the whole simulated volume. For the hyperfine-mediated interaction we averaged over 10^6 randomly generated spin configurations within the whole volume. The simulation was done for 100 different configurations of nuclear spins to account for initial state dependence of the decoherence process. The results were checked for convergence with changing parameters of the model.

For the electron spin free induction decay the real parts of different diagrams, Figs. 2,9, averaged over spatial and spin configurations of ^{29}Si are shown in Fig. 10. At very short times $t < \max\{A^{\rm hf}\}^{-1}$ the second order terms[25] are $V_2^{\rm hf} \sim t^2$, and $V_2^{\rm dd} \sim t^4$. In Fig. 10(a) we show the crossover from the short-time behavior to an intermediate regime with time dependencies $V_2^{\rm hf} \sim t^1, V_2^{\rm dd} \sim t^{2.3}$. The dispersions in the exponent at intermediate timescale is $\sim 5\%$ depending on spatial positions of ^{29}Si near the P donor and different initial configurations of nuclear spins. It also include errors due to a finite simulated volume. Unlike the electron spin in a quantum dot[25] the short-to-intermediate regime crossover in Si:P is more noticeable because of the stronger confinement and inhomogeneity of the electron wave function. For external magnetic fields $H < 0.1-1T$ the hyperfine-mediated term determines short-time spin dynamics, see Fig. 10(a). However, it can be efficiently suppressed by increasing the field. Moreover, it cancels completely in the spin echo. All the dipole-dipole fourth order terms develop on the timescale of the order of several msec, Fig. 10(b). However, on this timescale the electron spin coherence is completely destroyed by the $\langle V_2 \rangle$ term. This slow development of high order spin correlations is consistent with an experimental

measurements.[32] At a very short times the fourth order terms are $\sim t^6$ (not shown in the figures). This dependence changes to $V_4^{\mathrm{dd}} \sim t^{4.2}$ at longer timescale. The contribution of the four-spin diagram is about an order of magnitude larger than other fourth order terms. However, we abstain from attributing it to $1/Z$ expansion because there is no such difference between two and three-spin-fourth order terms. Probably, this is because the studied system of nuclear spins is dilute and Z is of order of unity. In Fig. 11 we show the total second and fourth order contributions (see inset) in the exponent for FID and spin echo setups. One can see that a π-pulse reduces electron spin decoherence. This effect is an analog of suppression of a spectral diffusion considered in phenomenological models.[42,59]

For the spin echo setup we obtain the time dependence of V_2^{dd} term comparable to that was calculated in Ref. 27. However, the fourth order terms in our model do not show the non-monotonic behavior.

We emphasize that in the Si:P system the non-contact hyperfine coupling between the electron and nuclear spins, not considered here, produces noticeable effects on electron spin dynamics.[44,45,46] To suppress these effects a high external magnetic field is required.[47] Moreover, in spin echo measurements on macroscopic samples the dipole-dipole interaction between electron spins causes an instantaneous diffusion.[9,60] This effect is beyond the scope of this paper on a single electron spin. For comparison with the experimental results given in Ref. 9, we account for the instantaneous diffusion with a phenomenological exponential decay, $e^{-t/t_{ID}}$. In the simulation we take the phenomenological relaxation time for instantaneous diffusion to be $t_{ID} = 1.1$ msec, obtained in Ref. 9. The results are shown in Fig. 12. Besides the echo modulations due to non-contact dipole-dipole interaction observed in the experiments we still have a moderate discrepancy. Because the magnetic field used in the experiment was of the order of 0.3 T, the contribution of the hyperfine-mediated terms should be small on the timescale of the echo decay (0.1-0.5 msec). We attribute this discrepancy to the effective mass approximation for the electron wave function. More detailed comparison should be done after echo modulation and instantaneous diffusion effects are accounted for by the theory. We leave it for further studies.

V. CONCLUSION

We developed a field theoretic approach to evaluate dynamics of an electron spin interacting with a nuclear spin bath in a high field regime. The approach provides a better understanding of the difference between stochastic models of an electron spin spectral diffusion and dynamic models of spin decoherence in the presence of the nuclear spin bath. It also throws light on the problem of reversibility of spin dynamics. The approach is based on a conventional diagrammatic technique utilized in the study of Heisenberg ferromagnets. The scheme allows for analytical evaluation of different processes contributing to the electron spin evolution. We show that electron spin dynamics in a nuclear spin environment can be factorized into a free precession in the Overhauser field and more complex dynamics due to an electron-nuclear spin entanglement. The latter can be evaluated using a linked cluster expansion procedure. The exact analytical expressions for second order and some high order processes are given. We show that spin decoherence of a P donor electron in a single Si crystal is mostly controlled by nuclear spin pair excitations at sufficiently low temperature and high magnetic field. Contributions of high order processes are small and can be neglected on a timescale up to several msec. A magnetic π-pulse flipping electron spin slows down the decoherence process. The simulated results are in fairly good agreement with experimental measurements of spin echo in macroscopic samples.

APPENDIX A

We briefly summarize the spin diagrammatic rules. Unlike Ref. 37 where the formalism was used for a statistically mixed state, our brackets correspond to a pure state specified by initial conditions. Averaging over a thermal ensemble in our case would mix dynamical contributions of electron-nuclear spin entanglement with effects of statistical distribution of Overhauser fields. For the sake of simplicity here we assume that $I = 1/2$. However, the approach can be extended to a more general case.[39]

The matrix element in Eq. (8) can be written as a product of brackets corresponding to single sites. At each nuclear spin site j with a given initial state, $|j\rangle$ $(= |\uparrow\rangle$ or $|\downarrow\rangle)$, an

expectation value of time ordered spin operators,

$$\langle j|T\{I^\alpha(t_1)I^-(t_2)...I^+(t_k)I^\beta(t_{k+1})...I^\mu(t_m)\}|j\rangle \tag{A1}$$

is zero if numbers of I^+ and I^- operators are not equal. Otherwise, we evaluate it with the Wick's theorem.[37] Using the spin commutation relations, $[I^-, I^+] = -2I^z$ and $[I^z, I^+] = I^+$ the bracket (A1) is transformed to the form where an operator I^+ (I^- would serve as well) is in the first position

$$\langle j|\overbrace{I^\alpha(t_1)I^+}(t)I^\beta(t_2)|j\rangle = \langle j|[I^\alpha(t_1), I^+(t)]I^\beta(t_2)|j\rangle + \langle j|I^+(t)I^\alpha(t_1)I^\beta(t_2)|j\rangle \tag{A2}$$

or in the last position

$$\langle j|I^\alpha(t_1)\overbrace{I^+(t)I^\beta}(t_2)|j\rangle = -\langle j|I^\alpha(t_1), [I^\beta(t_2), I^+(t)]|j\rangle + \langle j|I^\alpha(t_1)I^\beta(t_2)I^+(t)|j\rangle. \tag{A3}$$

Depending on the initial state operator, I^+ is moved to the right if $|j\rangle = |\uparrow\rangle$ or to the left if $|j\rangle = |\downarrow\rangle$. After applying

$$\begin{aligned} I^+(t)|\uparrow\rangle &= 0, \\ \langle\downarrow|I^+(t) &= 0. \end{aligned} \tag{A4}$$

a product of m spin operators is expanded into a sum of products of $m-1$ operators. This procedure is repeated until only a product of I^z operators is left. The latter term is evaluated directly. As a result, the bracket (A1) can be written in terms of all possible contractors of I^+ operator with I^- and I^z using

$$[I^\alpha(t_1), I^+(t)] = e^{i\omega(t-t_1)}[I^\alpha, I^+]_{t_1}, \tag{A5}$$

where the latter commutator is taken at time t_1. Unlike contractions of bosons or fermions a commutator of I^+ and either I^- or I^z is an operator that can be used in a next pairing. For example, in

$$\overbrace{I^+(t)\overbrace{I^z(t_1)}I^-}(t_2) \tag{A6}$$

the operator $I^+(t)$, firstly, is paired with $I^z(t_1)$ with resulting $I^+(t_1)$ operator paired with $I^-(t_2)$. Another specific example of spin pairing is a locked term.[37] In

$$\overbrace{I^+(t)I^-}^{}\overbrace{(t_1)I^+(t')I^-(t_2)}^{}, \tag{A7}$$

the operator $I^+(t)$ is paired with $I^-(t_1)$, then $I^+(t')$ is paired with the resulting operator $I^z(t_1)$ and finally with $I^-(t_2)$. By the locked term here we mean a term that contains an operator I^- with three contracting lines. The role of such terms in LCE we discuss in Appendix B.

In diagrams we depict I^+ vertices by points, I^- and I^z vertices by open circles and interaction terms by wavy lines. The Green's function, defined as

$$K_j(t_1, t_2) = \frac{\langle j|T\{I^+(t_1)I^-(t_2)\}|j\rangle}{(-2)\langle j|I_j^z|j\rangle} = e^{i\omega_j(t_1-t_2)}\{\delta_{j\downarrow}\theta(t_2 - t_1) - \delta_{j\uparrow}\theta(t_1 - t_2)\}, \tag{A8}$$

is shown as a line with an arrow propagating from I^+ to I^-. An initial spin state determines Green's function time evolution. One can see that the Green's function propagates back in time (arrow points opposite to the time arrow) if the initial spin state is $\uparrow$, and forward in time, if the state is $\downarrow$. Although I^- and I^z vertices are depicted by same symbols there is a topological difference in their appearance in diagrams. I^z vertex can be either separated from any Green's function or connected to one incoming and one outgoing Green function. I^- vertex can have one incoming line or two incoming and one outgoing lines. I^+ vertex always has one outgoing Green function line. For interactions, a wavy line connecting two circles corresponds to $I^z I^z$ term, while a line connecting a point and a circle corresponds to I^+I^- term.

The diagram representation can be easily translated into Green's functions. For example, the second order flip-flop term, Fig. 2 can be written as

$$\langle V_2 \rangle = A \sum_{i=\uparrow, j=\downarrow} B_{ij}^2 \int_0^t dt_1 \int_0^t dt_2 K_i(t_1, t_2) K_j(t_2, t_1)(-2)^2 \langle i|I_i^z|i\rangle\langle j|I_j^z|j\rangle. \tag{A9}$$

The coefficient A in front of the sum accounts for a number of equivalent diagrams. In the particular case it is equal one. The coefficient $(-2)^2$ appears from two contractions of I^+I^- operators. Analytical expressions for diagrams are dependent on initial spin states. For

example, pairs ↑↑ or ↓↓ give zero contribution to $\langle V_2 \rangle$ term, see Fig. 2, while contribution of ↑↓ and ↓↑ pairs are equal. We usually omit this configuration dependence in graphic representation. For example, three spin diagram, Fig. 3(c) corresponds to two possible spin clusters ↑↓↓ and ↓↑↑ (Fig. 13) that have different analytical expressions. In general, one can distinguish between configurations that can be transformed to each other by changing order in spin counting or by rotation or inversion of the coordinate system and configurations that are distinct. First type of configurations are ↑↓↓ and ↓↑↓. If we start counting spins from the ↑ site these configurations are the same, and they have equal analytical expressions. In the case given in Fig. 13 the two spin configurations are connected by the inversion operation. An analytical form of the second diagram at the right hand side can be obtained by changing signs at all frequencies ω in an expression for the first diagram. Distinct configurations are, for example, ↑↓↑↓ and ↑↑↓↓ contributing to the same forth order ring diagram, Fig. 3(f).

APPENDIX B

Here we consider in more details a physical origin of locked terms in LCE. For the sake of simplicity we assume that the interaction is

$$V(t) = \sum_{ij} B_{ij} I_i^+(t) I_j^-(t), \tag{B1}$$

and we evaluate

$$\langle n|T\{e^{-i\int_0^t V(t')dt'}\}|n\rangle = \langle n|1 + (-i)\int_0^t V(t')dt' + (-i)^2/2! \int_0^t \int_0^t T\{V(t')V(t'')\}dt'dt'' + ...|n\rangle, \tag{B2}$$

where n denotes a spin configuration. The locked diagrams appear in the fourth order contribution and correspond to two-spin and three-spin excitations. A two-spin-fourth-order correction can be written as

$$3(-i)^4/4! \sum_{ij} B_{ij}^4 \int_0^t \int_0^t \int_0^t \int_0^t T\{\langle i|I_i^+(t_1)I_i^-(t_2)I_i^+(t_3)I_i^-(t_4)|i\rangle \tag{B3}$$

$$\langle j|I_j^-(t_1)I_j^+(t_2)I_j^-(t_3)I_j^+(t_4)|j\rangle\}dt_1dt_2dt_3dt_4,$$

where we have separated operators corresponding to different spins. The coefficient 3 in front of Eq. (B3) accounts for possible choices of i and j. Eq. (B3) is nonzero only if $i = \uparrow, j = \downarrow$ (for $i = \downarrow, j = \uparrow$ we just change order in counting of spins and get the same configuration). The only possible time ordering in this case is $t_1 > t_2 > t_3 > t_4$ or $t_1 > t_4 > t_3 > t_2$. The integrand for both sets of time ordering is the same and equal $e^{i\omega_{ij}(t_1-t_2+t_3-t_4)}$. The same result we can get with the spin diagram technique and diagram equations given in Fig. 8. Firstly, we expand the time ordered product of spin operators in Eq. (B3) in terms of all possible contractors as discussed in Appendix A. There are two unlinked terms of the form

$$I_i^+(t_1)I_i^-(t_2)I_i^+(t_3)I_i^-(t_4)I_j^-(t_1)I_j^+(t_2)I_j^-(t_3)I_j^+(t_4), \tag{B4}$$

two linked terms corresponding to the ring diagram, given in Fig. 4(f)

$$I_i^+(t_1)I_i^-(t_2)I_i^+(t_3)I_i^-(t_4)I_j^-(t_1)I_j^+(t_2)I_j^-(t_3)I_j^+(t_4), \tag{B5}$$

eight single-site locked terms, Fig. 4(g), of the form

$$I_i^+(t_1)I_i^-(t_2)I_i^+(t_3)I_i^-(t_4)I_j^-(t_1)I_j^+(t_2)I_j^-(t_3)I_j^+(t_4), \tag{B6}$$

and four two-sites locked terms, Fig. 4(h)

$$I_i^+(t_1)I_i^-(t_2)I_i^+(t_3)I_i^-(t_4)I_j^-(t_1)I_j^+(t_2)I_j^-(t_3)I_j^+(t_4). \tag{B7}$$

Eq. (B4) corresponds to the series expansion of the second order contribution. However, it allows some non-physical states, because the contractions in it specify time ordering $t_1 > t_2$ and $t_3 > t_4$ only. By direct evaluation, one can show that the locked terms, Eqs. (B6,B7), modify it according to the diagram equation given in Fig. 8(a) to get a correct time ordering $t_1 > t_2 > t_3 > t_4$. It is a correction of overlapping of spin excitations discussed in Refs. 25,27. The locked diagram is the price we pay to obtain LCE for spins. This shows that the procedure to get an exponential form of a qubit decoherence is not as transparent as it was suggested in Ref. 27.

APPENDIX C

Here we provide explicit analytical expressions for two and three spin diagrams given in Fig. 9. The first term is denoted as V_{43}, the three-spin part of the second term is V_{41l} and the two-spin part of the second term plus the third term is V_{42l}. We do not include the coefficients $1/2$ indicated in Fig. 9. The analytical expression for the last, four-spin, diagram is lengthy though its evaluation is not complicated. We give terms for the hyperfine-mediated and dipole-dipole interactions separately.

Contributions of the hyperfine-mediated interaction are:

a) the three spin ring with overlapping corrected,

$$\langle V_{43}^{\text{hf}} \rangle = -\sum_{\uparrow\downarrow\downarrow} B_{ij}^2 B_{jk}^2 \{ 2it(\frac{1}{\omega_{ij}^2\omega_{ik}} + \frac{e^{2i\omega_{ij}t}}{\omega_{ij}^2\omega_{jk}}) + 2\frac{1 - e^{2i\omega_{ij}t}}{\omega_{ij}^3\omega_{jk}} + \frac{1 - e^{2i\omega_{ik}t}}{\omega_{ik}^2\omega_{jk}^2} - \frac{1 - e^{2i\omega_{ij}t}}{\omega_{ij}^2\omega_{jk}^2} \}, \quad \text{(C1)}$$

b) the diagram compensating a single site overlapping,

$$\langle V_{4l1}^{\text{hf}} \rangle = 2\sum_{\uparrow\downarrow\downarrow} B_{ij}^2 B_{ik}^2 \{ 2it\frac{1 + e^{2i\omega_{ij}t}}{\omega_{ij}^2\omega_{ik}} + \frac{(2\omega_{ik}^2 - \omega_{ij}\omega_{ik} + \omega_{ij}^2)(1 - e^{2i\omega_{ij}t})}{\omega_{ij}^3\omega_{ik}^2\omega_{jk}}$$
$$- \frac{1 - e^{2i(\omega_{ik} + \omega_{ij})t}}{2\omega_{ik}^2\omega_{ij}^2} \} + \{j \leftrightarrow k\}, \quad \text{(C2)}$$

c) the compensation of a double site overlapping (two diagrams),

$$\langle V_{4l2}^{\text{hf}} \rangle = -\sum_{\uparrow\downarrow} B_{ij}^4 \{ -2it\frac{1 + 2e^{2i\omega_{ij}t}}{\omega_{ij}^3} + \frac{e^{4i\omega_{ij}t} + 2e^{2i\omega_{ij}t} - 5}{2\omega_{ij}^4} \}. \quad \text{(C3)}$$

The same diagrams for dipole-dipole interaction only have the following expressions:

a) the three spin ring with overlapping corrected,

$$\langle V_{43}^{\text{dd}} \rangle = -\sum_{\uparrow\downarrow\downarrow} B_{ij}^2 B_{jk}^2 \{ 2it(\frac{2\omega_{ik} - \omega_{ij}}{\omega_{ij}^2\omega_{ik}\omega_{jk}} - \frac{(1 - e^{i\omega_{ij}t})^2}{\omega_{ij}^2\omega_{jk}}) + 4\frac{(\omega_{ij}^2 - 2\omega_{jk}^2)e^{i\omega_{ij}t}}{\omega_{ij}^3\omega_{ik}\omega_{jk}^2}$$
$$- \frac{e^{2i\omega_{ik}t}}{\omega_{ik}^2\omega_{jk}^2} - 4\frac{e^{i\omega_{ik}t}}{\omega_{ij}\omega_{ik}\omega_{jk}^2} - \frac{(3\omega_{ij} - 2\omega_{jk})e^{2i\omega_{ij}t}}{\omega_{ij}^3\omega_{jk}^2} + 4\frac{e^{i(\omega_{ik} + \omega_{ij})t}}{\omega_{ij}\omega_{ik}\omega_{jk}^2} + \frac{\omega_{ij} + 6\omega_{ik}}{\omega_{ik}^2\omega_{ij}^3} \}, \quad \text{(C4)}$$

b) the diagram compensating a single site overlapping,

20

$$\langle V_{4l1}^{\mathrm{dd}} \rangle = 2 \sum_{\uparrow\downarrow\downarrow} B_{ij}^2 B_{ik}^2 \{ 2it \frac{2 - (1 - e^{i\omega_{ij}t})^2}{\omega_{ij}^2 \omega_{ik}} - \frac{12 e^{i(\omega_{ij}+\omega_{ik})t} + e^{2i(\omega_{ij}+\omega_{ik})t} - 8e^{i(\omega_{ik}+2\omega_{ij})}}{2\omega_{ij}^2 \omega_{ik}^2}$$

$$+ \frac{8(\omega_{ij}^2 + \omega_{ik}^2 - \omega_{ij}\omega_{ik})e^{i\omega_{ij}t} - (2\omega_{ik}^2 + 3\omega_{ij}^2 - 3\omega_{ij}\omega_{ik})e^{2i\omega_{ij}t}}{\omega_{ij}^3 \omega_{ik}^2 (\omega_{ij} - \omega_{ik})}$$

$$+ \frac{6\omega_{ij}^2 + \omega_{ij}\omega_{ik} + 6\omega_{ik}^2}{2\omega_{ij}^3 \omega_{ik}^3} \} + \{ j \leftrightarrow k \}, \tag{C5}$$

c) the compensation of a double site overlapping,

$$\langle V_{4l2}^{\mathrm{dd}} \rangle = -\sum_{\uparrow\downarrow} B_{ij}^4 \{ 2it \frac{2(1 - e^{i\omega_{ij}t})^2 - 3}{\omega_{ij}^3} + \frac{e^{4i\omega_{ij}t} - 8e^{3i\omega_{ij}t} + 12e^{2i\omega_{ij}t} + 8e^{i\omega_{ij}t} - 13}{2\omega_{ij}^4} \}. \tag{C6}$$

In equations $\{ j \leftrightarrow k \}$ means the same expression with interchanged j and k indexes.

ACKNOWLEDGMENTS

---

[*] ssaikin@physics.ucsd.edu; http://www.physics.ucsd.edu/~ssaikin/

[1] A. Schweiger and G. Jeschke, *Principles of pulse electron paramagnetic resonance* (Oxford University press, New York, 2001).

[2] M. A. Nielsen and I. L. Chuang, *Quantum computation and quantum information* (Cambridge Univ. press, Cambridge, 2000).

[3] S. A. Wolf, A. Y. Chtchelkanova, D. M. Treger, IBM J. Res. & Dev. **50**, No. 1, 101 (2006).

[4] K. Ono and S. Tarucha, Phys. Rev. Lett. **92**, 256803 (2004).

[5] M. V. G. Dutt, J. Cheng, B. Li, X. Xu, X. Li, P. R. Berman, D. G. Steel, A. S. Bracker, D. Gammon, S. E. Economou, R.-B. Liu, and L. J. Sham Phys. Rev. Lett. **94**, 227403 (2005).

[6] A. C. Johnson, J. R. Petta, J. M. Taylor, A. Yacoby, M. D. Lukin, C. M. Marcus, M. P. Hanson, A. C. Gossard, Nature **435**, 925 (2005).

[7] P.-F. Braun, X. Marie, L. Lombez, B. Urbaszek, T. Amand, P. Renucci, V. K. Kalevich, K. V. Kavokin, O. Krebs, P. Voisin, Y. Masumoto, Phys. Rev. Lett. **94**, 116601 (2005).

[8] R. Giraud, W. Wernsdorfer, A. M. Tkachuk, D. Mailly, B. Barbara, Phys. Rev. Lett. **87**, 057203 (2001).

[9] A. M. Tyryshkin, J. J. L. Morton, S. C. Benjamin, A. Ardavan, G. A. D. Briggs, J. W. Ager, S. A. Lyon, J. Phys.: Condens. Matter **18**, S783 (2006).

[10] L. Viola, E. Knill, and S. Lloyd, Phys. Rev. Lett. **82**, 2417 (1999).

[11] A. M. Steane, Phys. Rev. A **68**, 042322 (2003).

[12] J. R. Klauder and P. W. Anderson, Phys. Rev. **125**, 912 (1962).

[13] M. Chiba and A. Hirai, J. Phys. Soc. Jpn. **33**, 730 (1972).

[14] K. M. Salikhov, A. G. Semenov, Yu. D. Tsvetkov, *Electron Spin Echo and its Application* (Nauka, Novosibirsk, 1976) (In Russian).

[15] N. Prokof'ev and P.C.E. Stamp, Rep. Prog. Phys. **63**, 669 (2000).

[16] A. V. Khaetskii, D. Loss, and L. Glazman, Phys. Rev. Lett. **88**, 186802 (2002).

[17] I. A. Merkulov, Al. L. Efros, and M. Rosen Phys. Rev. B **65**, 205309 (2002).

[18] S. Saykin, D. Mozyrsky, and V. Privman, Nano Letters **2**, 651 (2002).

[19] J. Schliemann, A. Khaetskii, and D. Loss, J. Phys., Condens. Matter **15**, R1809 (2003).

[20] Yu. V. Pershin and V. Privman, Nano Letters **3**, 695 (2003).

[21] S. I. Erlingsson and Y. V. Nazarov Phys. Rev. B **70**, 205327 (2004).

[22] W. A. Coish and D. Loss, Phys. Rev. B **70**, 195340 (2004).

[23] W. M. Witzel, R. de Sousa, and S. Das Sarma, Phys. Rev. B **72**, 161306(R) (2005).

[24] N. Shenvi, R. de Sousa, and K. B. Whaley, Phys. Rev. B 71, 144419 (2005).

[25] W. Yao, R.-B. Liu, and L. J. Sham, e-print cond-mat/0508441 (2005).

[26] K. A. Al-Hassanieh, V. V. Dobrovitski, E. Dagotto, B. N. Harmon, e-print cond-mat/0511681.

[27] W. M. Witzel and S. Das Sarma, Phys. Rev. B **74**, 035322 (2006).

[28] W. Yao, R.-B. Liu, and L. J. Sham, e-print cond-mat/0604634. (2006)

[29] C. Deng and X. Hu, Phys. Rev. B **73**, 241303(R) (2006).

[30] V. Privman, J. Statistical Phys. **110**, 957 (2003).

[31] W.-K. Rhim, A. Pines, and J. S. Waugh, Phys. Rev. Lett. **25**, 218 (1970).

[32] H. Cho, T. D. Ladd, J. Baugh, D. G. Cory, C. Ramanathan, Phys. Rev. B **72**, 054427 (2005).

[33] R. B. Stinchcombe, G. Horwitz, F. Englert, and R. Brout, Phys. Rev. **130**, 155 (1963).

[34] B. Giovannini and S. Koide, Prog. Theor. Phys. **34**, 705 (1965).

[35] Y. L. Wang, S. Shtrikman, and H. Callen, Phys. Rev. **148**, 419 (1966).

[36] V. G. Vaks, A. I. Larkin, and S. A. Pikin, Zh. Eksp. Teor. Phys. **53**, 1089 (1967) [Sov. Phys. JETP **26**, 647 (1968)].

[37] Yu. A. Izyumov and F. A. Kassan-Ogly, Fiz. Met. Metalloved. **26**, 385 (1968); **30**, 225 (1970).

[38] Yu. A. Izyumov, F. A. Kassan-Ogly, and Yu. N. Scryabin, *Field Methods in Theory of Ferromagnetism* (Fiziko-Matematicheskaya Literatura, Moscow, 1974) (in Russian).

[39] David Hsing-Yen Yang and Yung-Li Wang, Phys. Rev. B **10**, 4714 (1974).

[40] V. G. Baryakhtar, V. N. Krivoruchko, and D. A. Yablonskii, Teoret. and Matem. Fizika **56**, 149 (1983) [Theor. and Math. Phys. **56**, 731 (1983)].

[41] V. G. Baryakhtar, V. N. Krivoruchko, and D. A. Yablonskii, *Green Functions in the Theory of Magnetism* (Nauk-dumka, Kiev, 1984) (in Russian).

[42] C. P. Slichter, *Principles of Magnetic Resonance* (Springer-Verlag, Berlin, 1980).

[43] L. G. Rowan, E. L. Hahn, and W. B. Mims, Phys. Rev. **137**, A61, (1965).

[44] M. Fanciulli, P. Hofer, and A. Ponti, Physica B **340-342**, 895 (2003).

[45] J. J. L. Morton, A. M. Tyryshkin, A. Ardavan, K. Porfyrakis, S. A. Lyon, G. A. D. Briggs, J. Chem. Phys. **122**, 174504 (2005).

[46] E. Abe, K. M. Itoh, J. Isoya, and S. Yamasaki, Phys. Rev. B **70**, 033204 (2004).

[47] S. Saikin and L. Fedichkin, Phys. Rev. B **67**, 161302 (2003).

[48] N. G. van Kampen, *Stochastic Processes in Physics and Chemistry* (Elsevier North-Holland, Amsterdam 2001).

[49] G.D. Mahan, *Many-Particle Physics* (Kluwer Academic/Plenum Publishers, New York, 2000).

[50] A. A. Abrikosov, L. P. Gorkov, I. E. Dzyaloshinski *Methods of quantum field theory in statistical physics* (Prentice-Hall Inc., Englewood Cliffs, New Jersey 1963).

[51] L. P. Kadanoff and G. Baym, *Quantum statistical mechanics; Green's function methods in equilibrium and nonequilibrium problems* . (New York, W. A. Benjamin, 1962)

[52] L. V. Keldysh, Sov. Phys. JETP **20**, 1018 (1965), [Zh. Eksp. Teor. Fiz. **47**,1515 (1964)].

[53] G. Feher, Phys. Rev. **114**, 1219 (1959).

[54] W. H. Furry, Phys. Rev. **51**, 125 (1937).

[55] R. Brout, Phys. Rev. **118**, 1009 (1960).

[56] B.E. Kane, Nature **393**, 133 (1998).

[57] W. Kohn, *Solid State Physics*, vol. 5, 257 (1957).

[58] D. Stepanenko, G. Burkard, G. Giedke, A. Imamoglu, Phys. Rev. Lett. **96**, 136401 (2006).

[59] E. L. Hahn, Phys. Rev. **80**, 580 (1950).

[60] A. Ferretti, M. Fanciulli, A. Ponti, A. Schweiger, Phys. Rev. B **72**, 235201 (2005).

FIGURE CAPTIONS:

Fig. 1: Schematic representation of two-branch evolution.

Fig. 2: Second order diagram corresponding to nuclear spin pair flip-flop processes.

Fig. 3: Set of third order diagrams

Fig. 4: Fourth order diagrams.

Fig. 5: Second order contribution to decoherence in LCE that includes a series of even orders of a conventional perturbation expansion.

Fig. 6: Renormalization of a Green's function by $I_i^z I_j^z$ interaction.

Fig. 7: Compensation of spin excitations overlapping in time by a locked diagram. Time overlap in one site (j).

Fig. 8: Compensation of spin excitations overlapping by a locked diagram. Time overlap in two sites (i and j).

Fig. 9: The total fourth order contribution of nuclear spin excitations to electron spin decoherence. The first diagram corresponds the ring propagation of spin excitation in three-spin clusters ↑↓↓ and ↓↑↑. The second, single-site locked, diagram corrects overlapping of excitations. It contributes spin dynamics of three and two-spin clusters as shown in Figs. 7 and 8. The third, two-site locked, diagram corrects overlapping of two spin excitations, Fig. 8. The last diagram describes four-spin ring excitations in spin clusters ↓↑↑↑, ↑↓↓↓, ↑↓↑↓ and ↑↑↓↓.

Fig. 10: Contributions of linked clusters to the electron spin decoherence: (a) Crossover from the short-time evolution to the intermediate regime. (b) Development of the fourth order terms in the intermediate time regime. V_2 corresponds to the spin pair flip-flop process in Fig. 2; V_{43} - the three-spin excitation, the first term in Fig. 9; V_{4l1} - the single site spin locked diagram, the three-spin part of the second term in Fig. 9; V_{4l2} - correction of overlapping of two-spin excitations given in the bracket in Fig. 8(a), and V_4 - the four-spin ring diagram, the last term in Fig. 9.

Fig. 11: Time dependence of second and fourth (inset) order terms in the exponent. FID vs. spin echo decay.

Fig. 12: Spin echo decay in comparison with the experimental data.[9] Orientation of the external magnetic field is along (100) direction in the crystallographic axes.

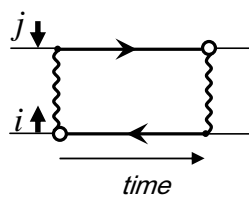Fig. 13: Representation of a third order diagram using cluster configurations.
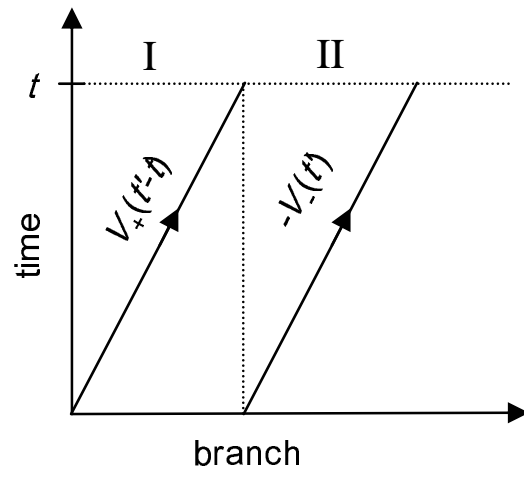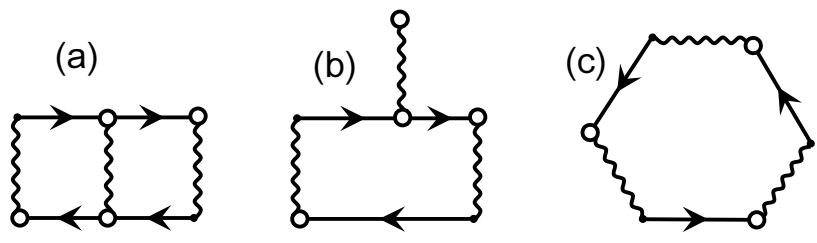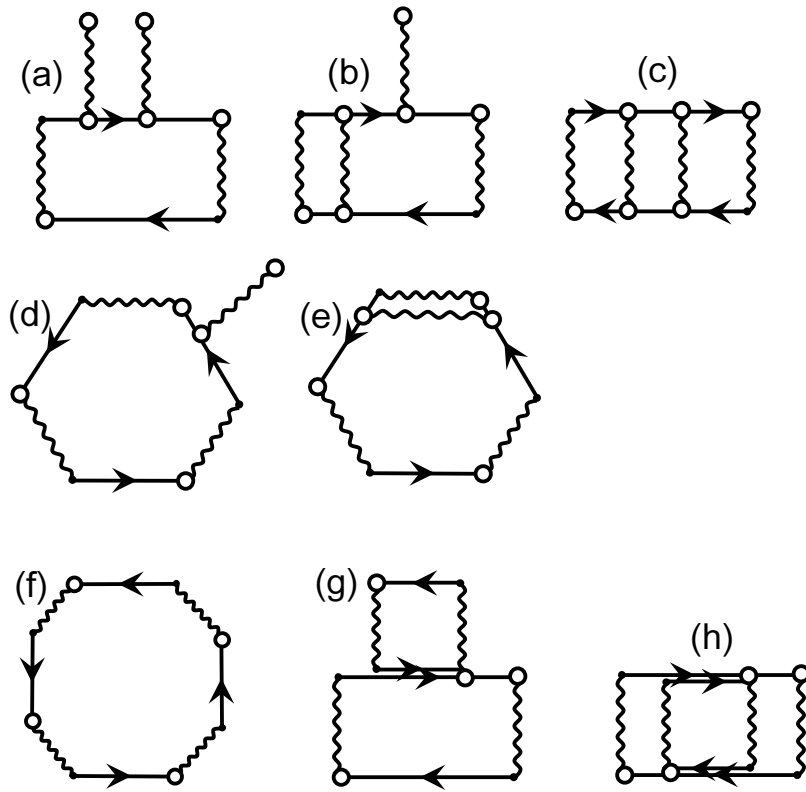
FIG. 1:

FIG. 2:

FIG. 3:

FIG. 4:

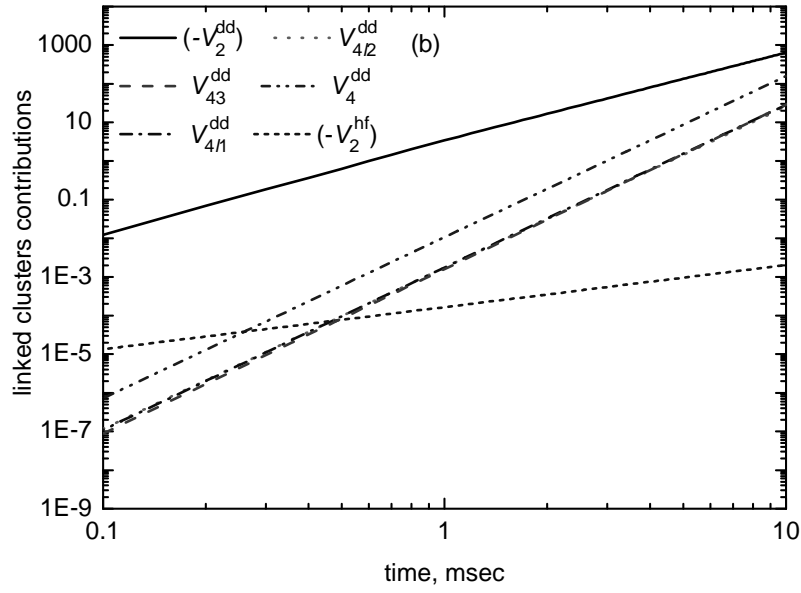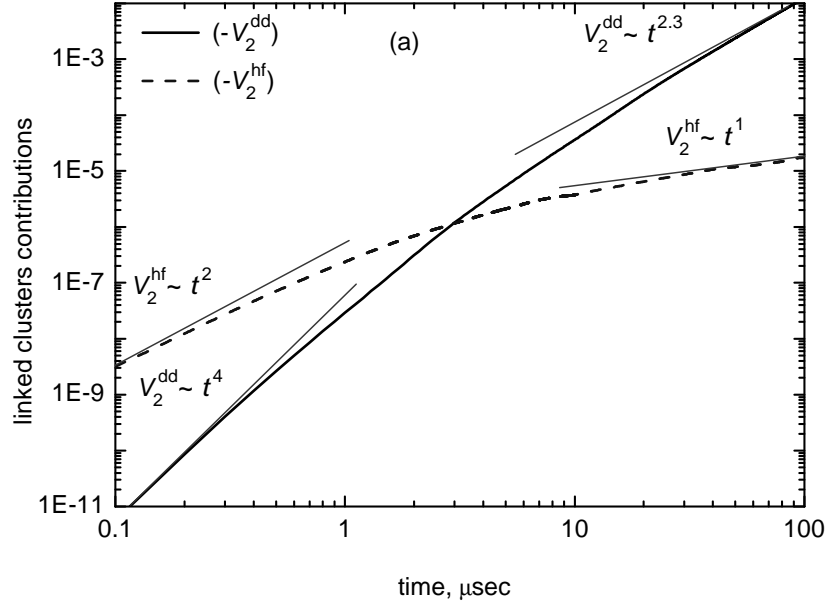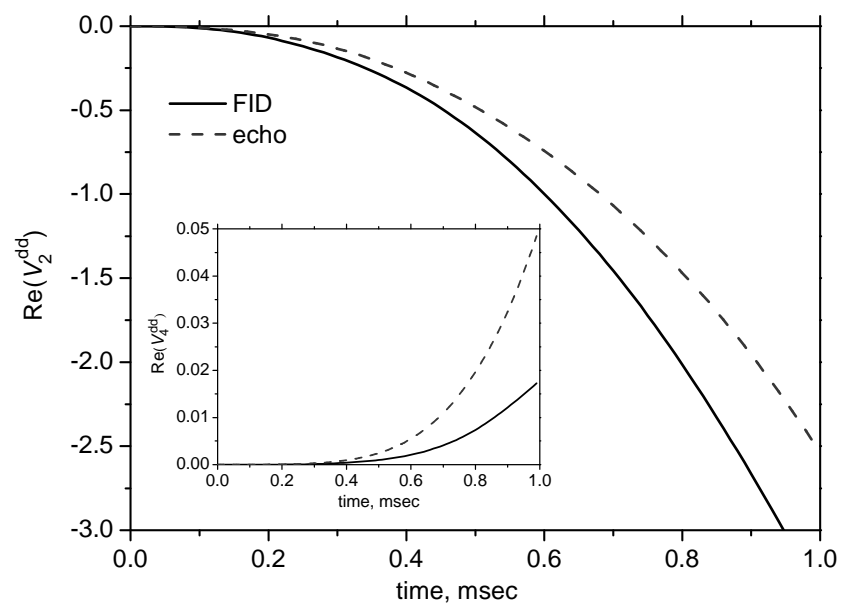$$e^{\,\square} \;=\; 1 + \square + (1/2!)\ \square\ \square + \ldots$$
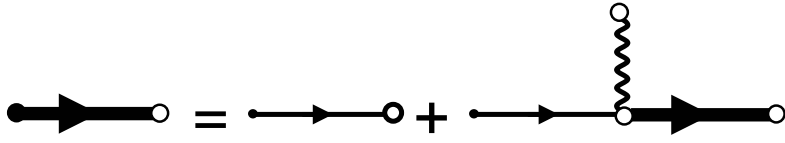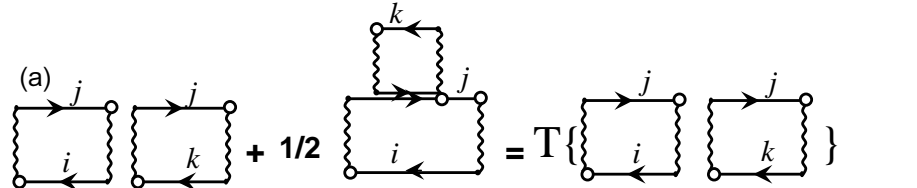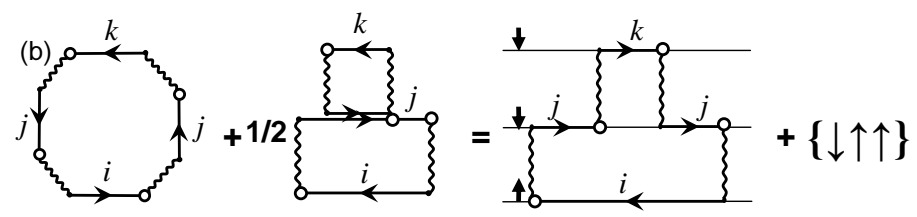
FIG. 5:

FIG. 6:

FIG. 7:

FIG. 8:

FIG. 9:

FIG. 10:

FIG. 11:

FIG. 12:

FIG. 13: